Astron. Astrophys. 358, 353–367 (2000)

ASTRONOMY AND ASTROPHYSICS

Angle dependent partial frequency redistribution in the interplanetary medium at Lyman α

E. Quémerais

Service d'Aéronomie du CNRS, B.P. 3, 91371 Verrières le Buisson, France (eric.quemerais@aerov.jussieu.fr)

Received 21 January 2000 / Accepted 31 March 2000

Abstract. We present here the results of a model of multiple scattering at Lyman α in the interplanetary medium. This paper uses the formalism of Angle Dependent Partial Frequency Redistribution which allows a computation of the actual line profile for a hydrogen velocity distribution taking into account actual local velocities and temperatures. This work extends the results of Quémerais & Bertaux (1993) which used the Complete Frequency Redistribution hypothesis and a constant velocity and temperature. Our computation also includes a scattering phase function and a realistic solar line profile. The radiative transfer computations are compared to the values obtained by various approximations in both the inner and the outer heliosphere. Correction tables are derived from these comparisons.

Key words: radiative transfer – Sun: UV radiation – inteplanetary medium – ultraviolet: solar system

1. Introduction

The existence of the interplanetary Lyman α background has been known for almost thirty years (Thomas & Krassa, 1971; Bertaux & Blamont, 1971). This phenomenon has been studied by many space instruments because it is a source of information on the interplanetary medium, the local interstellar medium, the solar wind and even, as it was shown lately, activity distribution on the solar disk (Bertaux et al., 1999b). Lists of previous space experiments studying the interplanetary hydrogen distribution can be found in Ajello et al. (1987) and Quémerais et al. (1994).

At the present time, we can divide the study of the Lyman α background into two main categories, photometric and spectroscopic, with different methods and applications. The first one is based on the intensity distribution observed over the whole sky. In the inner heliosphere, this allows to derive latitudinal variations of the solar wind mass flux distribution from remote sensing, a method which is complementary to the in-situ measurements of Ulysses (Bertaux et al., 1996). The SWAN instrument on the SOHO spacecraft, which was launched in December 1995, has been applying this technique quite successfully (Bertaux et al., 1997; Kyrölä et al., 1998). After 4 years of operations, the all-sky data recorded by the SWAN detectors show variations of the intensity pattern which are clearly due to the 11-year solar activity cycle (Bertaux et al., 1999a).

In the outer heliosphere, say outside 40 AU, the hydrogen distribution is not affected by solar EUV photo-ionization or charge exchange with solar wind protons as it is the case in the inner heliosphere. There, the H atoms are mainly influenced by the interface structure between the expanding solar wind and the ionized component of the interstellar medium. This interface, called the heliopause, is the object of many speculations concerning its nature, stability and actual position. For a review concerning this problem, see e.g. Baranov (1990). The neutral H atoms are coupled to the plasma components of the solar wind and of the interstellar medium through charge exchange processes. As a result, the outer heliosphere hydrogen distribution is substantially different from the case of the hot model where the H atom distribution is a simple gaussian distribution with constant number density far away from the sun (Thomas, 1978). One striking feature of the outer hydrogen atom distribution obtained by theoretical models including the effects of the heliospheric interface is the so-called hydrogen wall. This wall is due to a pile-up of neutral H atoms in the region where the instellar plasma is strongly heated and decelerated. Charge exchange between slowed down interstellar protons and neutral hydrogen atoms leads to a new neutral hydrogen component. It is characterized by a large temperature and a small bulk velocity in the solar frame (Baranov & Malama, 1993; Zank et al., 1996; Baranov et al., 1998). Since 1993, a series of observations have been performed by the UV Spectrometers on board the Voyager 1 and Voyager 2 spacecraft to try to observe the signature of the hydrogen wall in the Lyman α pattern (Quémerais et al., 1995). Hall et al. (1993) reported that the Lyman α intensity measured away from the sun was falling off with distance less quickly than expected from a standard hot model. This result suggested that there was a positive gradient of neutral hydrogen at large distance from the sun and could be explained by the existence of an interface region. However, the actual gradient observed by Hall et al. (1993) was not confirmed by later dedicated observations (Quémerais et al., 1995). An alternate explanation is now considered, i.e. that the increase of Lyman α intensity in the upwind direction could be partially due to a constant emission from HII regions in the galactic plane (Quémerais et al., 1995).

Send offprint requests to: E. Quémerais

This question is still unresolved and the latest data will need to be compared to the best modeling available.

Spectroscopic study of the interplanetary background is possible too. Recent experiments have measured the interplanetary Lyman α line profile and even more observations will be available in the future. The Goddard High Resolution Spectrometer on the Hubble Space Telescope has been used to measure the interplanetary Lyman α line profile (Clarke et al., 1995). Recently, Quémerais et al. (1999) have developed a new technique to derive interplanetary Lyman α line shifts by using the hydrogen absorption cell data obtained over one year by the SWAN instrument. The same data will also be used to measure linewidths, although in many cases it is necessary to estimate the UV stellar background observed by SWAN to get a correct measurement. This work is still ongoing. In the future, new spectrometers like the SCARI instrument (Chakrabarti et al., 1994, Stephan et al., 1998) will be flown either on rockets or on space missions and will provide precise measurements of the interplanetary Lyman α line profile.

The precise measurements obtained by the various space experiments mentioned above require now a precise modeling of this phenomenon if we want to be able to study these data correctly. The goal of this paper is to present a realistic modeling of the interplanetary Lyman α background by use of a detailed computation of the scattering process. The hydrogen velocity distribution will be taken as an input to our modeling but will not be discussed here. This paper uses the so-called *hot model* which does not take into account effects of the heliospheric interface in the outer heliosphere but has proved quite effective to describe the inner heliosphere (Thomas, 1978; Lallement et al., 1985; Pryor et al., 1992; Kyrölä et al., 1998).

In the previous literature, radiative transfer effects have not often been considered very precisely. The main reason is that in the inner heliosphere, the interplanetary medium is supposed to be optically thin at Lyman α. In such a case, one needs only to integrate the first scattering order over the line of sight to compute the scattered intensity. Unfortunately, this is not quite correct as shown by Keller et al. (1981) and confirmed by Hall (1992) and Quémerais & Bertaux (1993). Although the neutral hydrogen number density in the vicinity of the sun is small enough to have an optically thin medium, the number density increases with distance from the sun. At 10 AU from the sun, the medium is not optically thin anymore and second, or larger, scattering order photons have to be considered. Moreover, a fraction of the photons which are scattered at a larger distance can come back toward the sun and contribute to the inner heliosphere emission pattern. This phenomenon was clearly obtained by Keller et al. (1981), Hall (1992) and Quémerais & Bertaux (1993) which used different computation schemes.

Lallement et al. (1985) have used a more sophisticated approach than the previous one. They consider that the medium is not really optically thin and compute the optically thickness between the scattering point and the observer. While integrating on the line of sight to compute the intensity, the local emissivity at the scattering point is multiplied by an extinction term deduced from the optical thickness between the scatterer and the observer. This is called self-absorption because the same hydrogen atoms contributing to the emissivity on the line of sight also create this extinction, which is the source of high scattering order photons. This approach makes two important approximations. First, extinction between the sun and first scattering point is neglected. Second, the contribution of photons with a scattering order higher than one is neglected. Both terms are supposed to more or less compensate one another. We will see that this is not quite true in the next section.

A third approach has also been used previously (Scherer & Fahr, 1996). These authors compute the first order scattering component exactly, including extinction between the sun and the scattering point and also between the scattering point and the observer, but neglect all photons with a scattering order higher than one.

In what follows, we will call optically thin (O.T.) approximation the case where only first order scattering processes are included and no extinction, or self absorption, on the photon path is considered. We will call self absorption approximation (S.A.) the case where extinction between the scattering point and the observer is added and finally primary term approximation the case where extinction between the sun, the scattering point and the observer is used.

The works of Keller et al. (1981), Hall (1992) and Quémerais & Bertaux (1993) used the hypothesis of Complete Frequency Redistribution which assumes that there is no link between the frequencies of the photon before and after scattering. In that case, the emission profile at one point is simply defined by the local temperature of the hydrogen distribution and is independent of the incoming profile. This simplifying assumption was justified by the fact that these authors were only interested in the total number of scattered photons and not their actual frequency distribution. Moerover, they assumed that the interplanetary gas was isothermal with constant velocity from the sun. Finally, it was found easier to assume also that the solar Lyman α emission was *white*, which means that the source profile is flat. All these assumptions cancelled the possibility to have a correct representation of the interplanetary Lyman α line profile and justified the use of Complete Frequency Redistribution (C.F.R.). A more correct representation of the scattering process was used by Scherer & Fahr (1996). This is called Angle Dependent Partial Frequency Redistribution (A.D.P.F.R.) and was extensively described by Mihalas (1970).

However, these authors assumed that for the scattering orders higher than one the interplanetary hydrogen was isothermal. This was done to save computation time and has no physical justification.

The work presented here is a complement to the work of Quémerais & Bertaux (1993) which studied radiative transfer at Lyman α in the frame of the CFR hypothesis. Our present goal is to be able to study precisely interplanetary Lyman α line profiles obtained from SWAN on SOHO, GHRS/HST or any other future experiment which could resolve the interplanetary line profile. The hydrogen velocity distribution used here is deduced from the hot model in the axicylindrical case (isotropic ionizing fluxes from the sun) (Lallement et al., 1985). In each

point of the heliosphere the input distribution is defined by the local number density, the local velocity vector in the solar rest frame and the temperature measured on three axis of an orthoradial frame where the X axis is defined by the interstellar wind direction. This means that the local distribution is not gaussian because the temperature can be different on each axis. At large distance from the sun, the local distribution goes back to the assumed gaussian conditions in the interstellar medium. We have also included in our computations of all scattering orders, the scattering phase function of Brandt and Chamberlain (1959). It should be noted that the new expression for the Lyman α scattering phase function obtained by Brasken & Kyrölä (1998) is very close to the phase function expression used here. Finally, computations were made using two types of solar initial Lyman α profile, first the white or flat profile but also in the last section, the recent profile obtained in september 1996 by the SUMER instrument on SOHO (Lemaire et al., 1998). In this work we have limited our computations to the case of anti-radial or anti-solar line of sight. This means that the observer is looking away from the sun with the sun in its back.

The second section gives a quick presentation of the hydrogen model and of the equations the model is based upon. As in the work of Quémerais & Bertaux (1993), our computation method combines two different approaches, one being an iterative scheme on the scattering order, the second being a Monte Carlo simulation. Note also that the effect of the natural width of the H Lyman α transition line is not taken into account.

In the third section, we compare the results of the Monte-Carlo and the iterative scheme. This allows us to validate our approach. Then, we show why higher order scattering photons cannot be neglected to derive the interplanetary Lyman α background. This is quite obvious in the outer heliosphere but applies also at one AU, contrary to the conclusions of Scherer & Fahr (1996). We show also that the CFR and ADPFR hypotheses give very similar results in terms of backscattered intensity. The main advantage of ADPFR is that it allows the computation of the line profile which is not the case of CFR.

Our results are applied to compute intensity, line shift and linewidth as seen from 1 AU for different viewing geometries and for different sets of parameters. We compare these results with the values using the three main approximations, i.e. optically thin, self-absorption and primary term.

The same study is performed again for an observer going from 1 AU to 100 AU. The observer is going either in the upwind (as the Voyager 1 and 2 spacecraft) or in the downwind direction like in the case of the Pioneer 10 spacecraft.

2. Model presentation

2.1. Local hydrogen distributions

The hydrogen distributions used in this work are derived from the Hot Model (Thomas 1978, Lallement et al. 1985). This model assumes that the hydrogen distribution at large distance from the sun is unperturbed by the sun. In that case, the H atom distribution is given by a maxwellian distribution characterized by three values *at infinity*, i.e. where the solar influence can be neglected. These values are the number density, the bulk velocity and the temperature, respectively noted N_H, V_H and T_H. If there is no interaction between the interstellar hydrogen atoms and the heliospheric interface, then those three quantities correspond to the values in the interstellar medium. On the other hand, as shown by Baranov & Malama (1993), the existence of the heliospheric interface and the hydrogen/proton coupling by charge exchange can induce significant changes between the local conditions at 50 AU and the conditions of the interstellar gas. In what follows, we will consider various sets of parameters at infinity. Multiple scattering effects depend very much on the number density, meaning that the parameter N_H is the most important parameter in this study.

As the H atoms get closer to the sun, they are affected by the solar gravitational pull, which is an attractive force, but also by the repulsive effect of the radiation pressure. Both forces have the same dependence on distance from the sun. The ratio of radiation pressure over solar attraction, noted μ, is constant for a given solar Lyman α flux. It varies during the 11-year solar activity cycle roughly between 0.7 (attractive case) and 1.5 (repulsive case) (De Toma et al., 1996). In the vicinity of the sun, neutral hydrogen atoms are ionized by charge exchange with the solar wind protons or photo-ionized by EUV photons. The total ionization rate is characterized by its value at 1 AU. The inverse of this quantity is noted T_d and is defined as the mean lifetime of an hydrogen atom staying at one AU from the sun. Typical values of T_d vary between 1.0×10^6 s and 2.0×10^6 s (Pryor et al., 1992; Quémerais et al., 1996).

All local H atom velocity distributions are represented by non-maxwellian distributions. The distributions are referenced to the three directions defined as radial, orthoradial and perpendicular. For a point $[x, y, z]$, we define the radial, orthoradial and perpendicular vectors by

$$\begin{array}{lccccc} \boldsymbol{U_r} = & [& \cos\theta, & \sin\theta\cos\varphi, & \sin\theta\sin\varphi &] \\ \boldsymbol{U_\theta} = & [& -\sin\theta, & \cos\theta\cos\varphi, & \cos\theta\sin\varphi &] \\ \boldsymbol{U_\varphi} = & [& 0, & -\sin\varphi, & \cos\varphi &] \end{array}$$

where the angles θ and φ are defined by

$$\begin{aligned} \theta &= \operatorname{acos}\left(\frac{x}{\sqrt{x^2+y^2+z^2}}\right) \\ \varphi &= \operatorname{atan}(z, y). \end{aligned}$$

Along each of these directions, the local distribution is a zero mean gaussian with different temperatures. They are noted T_r, T_θ and T_φ, respectively.

In the local rest frame of a computation cell, the local velocity distribution projected on any direction $\boldsymbol{N}$ is a normal gaussian, i.e. with zero mean value, with temperature T_N defined by

$$T_N = (\boldsymbol{N}\cdot\boldsymbol{U}_r)^2 T_r + (\boldsymbol{N}\cdot\boldsymbol{U}_\theta)^2 T_\theta + (\boldsymbol{N}\cdot\boldsymbol{U}_\varphi)^2 T_\varphi. \quad (1)$$

2.2. Computation of the scattered profile

Let us consider an intensity $I(\nu)$ arriving at a point M of the heliosphere. This point is characterized by its number density D_M, mean local velocity relative to our frame of reference (Sun rest

frame) $\boldsymbol{V}_M$ and its local temperatures along the radial, orthoradial and perpendicular axes. This intensity arrives along a direction defined by $\boldsymbol{N}_1$ and is scattered along a second direction noted $\boldsymbol{N}_2$.

The incident intensity $I_M(\nu_{cell})$ along $\boldsymbol{N}_1$ is defined as the intensity profile arriving in M in the rest frame of the cell, i.e. in the frame where the mean velocity of the gas is equal to zero. This value is obtained by shifting the previous expression using the relation

$$\nu_{cell} = \nu \left(1 - \frac{\boldsymbol{V}_M \cdot \boldsymbol{N}_1}{c}\right). \quad (2)$$

From now on, we will use the following notations. We define a reference temperature T_{ref}, which can be the temperature of the gas at infinity. We find a reference thermal velocity V_{ref} and a reference Doppler width defined by

$$\Delta\nu_{ref} = \frac{\nu_0}{c} \times V_{ref} = \frac{\nu_0}{c} \times \sqrt{\frac{2\,k\,T_{ref}}{m_H}}. \quad (3)$$

We thus define the normalized frequency x_{sun} relative to the sun rest frame by

$$x_{sun} = \frac{\nu - \nu_0}{\Delta\nu_{ref}}. \quad (4)$$

The normalized frequency relative to the local rest frame is noted x. Eq. 2 becomes

$$x = x_{sun} - \frac{\boldsymbol{V}_M \cdot \boldsymbol{N}_1}{V_{ref}} = x_{sun} - \boldsymbol{v}_m \cdot \boldsymbol{N}_1 \quad (5)$$

where $\boldsymbol{v}_m$ is the local mean velocity relative to the Sun rest frame normalized to V_{ref}.

In the rest frame of the computation cell, we neglect the natural width of the Lyman α transition. This means that the absorption cross section is proportional to the velocity distribution projected on the direction $\boldsymbol{N_1}$. Indeed, a photon with a normalized frequency x_1 in the local rest frame can only be scattered by an atom with a velocity $\boldsymbol{v}_d$ verifying the following relation which is obtained by writing that the scattering atom sees the photon with a frequency equal to the Lyman α transition frequency in its own rest frame.

$$x_1 = \boldsymbol{v}_d \cdot \boldsymbol{N}_1. \quad (6)$$

The photon emitted in direction $\boldsymbol{N}_2$ will have a normalized frequency relative to the local rest frame noted x_2 following the equation

$$x_2 = \boldsymbol{v}_d \cdot \boldsymbol{N}_2. \quad (7)$$

Noting γ the angle between the directions $\boldsymbol{N}_1$ and $\boldsymbol{N}_2$, if they are not colinear. We can define a local orthonormal frame noted $[\boldsymbol{u_1}, \boldsymbol{u_2}, \boldsymbol{u_3}]$ where

$$\boldsymbol{u_1} = \boldsymbol{N_1} \quad (8)$$

$$\boldsymbol{u_2} = \frac{1}{\sin\gamma}\left(-\cos\gamma\,\boldsymbol{N_1} + \boldsymbol{N_2}\right) \quad (9)$$

$$\boldsymbol{u_3} = \frac{1}{\sin\gamma}\left(\boldsymbol{N_1} \times \boldsymbol{N_2}\right). \quad (10)$$

The velocity of the scattering atom is noted $\boldsymbol{v}_d = \Sigma_{i=1}^{3} v_i \boldsymbol{u_i}$. Eqs. 6 and 7 become

$$x_1 = v_1 \quad (11)$$

$$x_2 = x_1 \cos\gamma + v_2 \sin\gamma. \quad (12)$$

In the case where $\boldsymbol{N}_1$ and $\boldsymbol{N}_2$ are colinear, it is easy to see that the frequency is conserved for $\gamma = 0$ and opposite for $\gamma = \pi$.

In our model assumption, the velocity distribution along $\boldsymbol{N}_1$ is a gaussian distribution of zero mean value and temperature T_1. In a same manner, the velocity distribution along $\boldsymbol{u}_2$ is also a normal gaussian distribution. Eqs. 11 and following show that,

- The absorption profile in the local rest frame of the computation cell is proportional to a normal gaussian profile with a temperature equal to the temperature of the local velocity distribution projected on the incident direction.
- If the emergent direction is perpendicular to the incident direction, the scattered profile is a gaussian profile (Complete Frequency Redistribution).
- If the emergent and incident directions are colinear, the scattered profile is proportional to the incident profile multiplied by the cross section profile. (Coherent Scattering).
- For other scattering angles, the emitted profile is the sum of a coherent profile and a gaussian which temperature is defined by the direction perpendicular to the incident direction and contained inside the plane defined by both emergent and incident directions (Angle Dependent Redistribution).

2.3. Computation scheme

Our model computes the emissivity at a given point due to photons scattered at the order $n+1$ by integrating over the whole sky intensities due to photons of order of scattering n.

For a point M in the heliosphere of number density D_M, the intensity in its local rest frame received from a direction $\boldsymbol{N_1}$ within a solid angle $d\Omega$ and a normalized frequency interval is $I(x)\,dx\,d\Omega$. T_1 is the temperature of the local velocity distribution projected on the incident direction. The fraction of the incoming intensity ΔI_n scattered at point M is equal to

$$\Delta I_n = \sigma_0(T_1)\,exp\left(-x^2\frac{T_{ref}}{T_1}\right) \times D_M \times \left(I(x)\,dx\,d\Omega\right). \quad (13)$$

The total scattered intensity is obtained by integration over the frequency and the whole space.

The absorbed intensity ΔI_n is distributed over all spatial directions with the probability $\phi(\gamma)/4\pi$, where γ is the angle defined above and $\phi(\gamma)$ is the scattering phase function. Here, the scattering is isotropic then $\phi(\gamma) = 1$. With no new assumption, we can easily include any type of scattering functions.

From Eq. 11, we can compute the spectral profile of the fraction of the intensity scattered in a direction $\boldsymbol{N_2}$. T_2 is the temperature of the hydrogen distribution along the direction within the plane [$\boldsymbol{N_1}$,$\boldsymbol{N_2}$] and perpendicular to $\boldsymbol{N_1}$.

In that case, the fraction of intensity scattered at frequency within x_2 and $x_2 + dx_2$ is equal to

$$I(x_2)\, dx_2 = \frac{\phi(\gamma)}{4\pi}\, \Delta I_n\, exp\left(-x_2^2\, \frac{T_{ref}}{T_2}\right) \sqrt{\frac{T_{ref}}{T_2}}\, \frac{dx_2}{\sqrt{\pi}}. \quad (14)$$

The total emission profile is obtained by integration over all incident frequencies and all incident directions in space. The result of this computation is the profile in the local rest frame. To get the intensity in the sun rest frame, we must apply Eq. 5 backwards for direction $\boldsymbol{N}_2$.

2.4. Computation of the intensity along the line of sight

The intensity observed at a point M in a direction $\boldsymbol{U}$ at frequency ν per frequency unit is obtained by integration over the line of sight of the local emissivity multiplied by extinction between the point of emission and the observer.

$$I(\boldsymbol{r}, \boldsymbol{U}, \nu) = \int_0^\infty \varepsilon(\boldsymbol{r} + s\boldsymbol{U}, -\boldsymbol{U}, \nu)\, e^{-\tau_\nu(s)}\, ds. \quad (15)$$

The local emission in a direction $\boldsymbol{\Omega}$, which is the opposite of the direction of the line of sight, is computed using the scheme presented in the preceding paragraphs. However, the following approximation is applied to save computation time.

Let us call $\varepsilon(x, \boldsymbol{\Omega})$ the emissivity per normalized frequency unit and per solid angle in the local rest frame of the computation cell. The total emissivity, in photon per sec per cubic meter, is obtained by

$$\varepsilon_{tot} = \int_{4\pi} d\Omega \int_{-\infty}^{\infty} dx\, \varepsilon(x, \boldsymbol{\Omega}). \quad (16)$$

Note that the total local emissivity is equal to the term of Eq. 13 integrated over all incoming frequencies and directions. In the case where a non-isotropic scattering phase function is applied there is no linear relation between ε_{tot} and $\varepsilon(x, \boldsymbol{\Omega})$.

To compute the successive orders of scattering, we must integrate the emissivities over all spatial directions. This requires us to store the local emission profile in each direction of a spatial grid at each point of our computation grid thus demanding a huge amount of storage and computation time. To alleviate this problem we have chosen the following approximation. In the local rest frame of our grid, we compute the local emissivity in 3 directions which are the radial, orthoradial and perpendicular directions as defined in the previous paragraph and their opposite. Each profile is noted with index from 1 to 3. Finally, it appears from Eqs. 11 that the profiles emitted along two opposite directions will be symmetrical around zero in the local rest frame of the cell. We then have the following equation where the sign noted s_i is the sign of the projection of $\boldsymbol{\Omega}$ on the radial, orthoradial and perpendicular directions.

$$\begin{aligned}\varepsilon(x, \boldsymbol{\Omega}) \;=\; & (\boldsymbol{\Omega} \cdot \boldsymbol{U}_r)^2\, \varepsilon_1(s_1 x) + (\boldsymbol{\Omega} \cdot \boldsymbol{U}_\theta)^2\, \varepsilon_2(s_2 x) \\ & + (\boldsymbol{\Omega} \cdot \boldsymbol{U}_\varphi)^2\, \varepsilon_3(s_3 x). \end{aligned} \quad (17)$$

This expression is applied to estimate the local emissivity per normalized frequency unit and per solid angle integrated in Eq. 16.

3. Model results: Are R.T. and/or ADPFR necessary?

Keller et al. (1981) were the first authors who carefully computed the effects of multiple scattering for an observer at various distances from the sun and looking radially away from the sun. Their computations were based on a Monte-Carlo approach and used the assumption of Complete Frequency Redistribution. Their conclusions were very important for the study of the interplanetary Lyman α background. Indeed, they showed that even at 1 AU from the sun, where the H number density is very small, the optically thin approach does not apply. In the downwind cavity, they found an intensity ratio for multiple scattering over optically thin assumption equal to 1.35. These results were later confirmed independently by Hall (1992) and Quémerais & Bertaux (1993).

Following this result, various approaches have been adopted. The first one includes a correction to the optically thin computation derived from a comparison with a radiative transfer computation. This was done by Ajello et al. (1987) or Pryor et al. (1992). Usually this correction is computed for one set of parameters defining the hydrogen distribution assuming that the ratio of intensity from radiative transfer to intensity from optically thin approximation will not change too much with different hydrogen distributions.

The second approach used by Scherer & Fahr (1996) or Scherer et al. (1999) computes only the first scattering term. These authors then claim that all higher orders of scattering are negligible which is contradicted by the work of Keller et al. (1981), Hall (1992) and Quémerais & Bertaux (1993) which were obtained independently and the results of this work in the case of Angle Dependent Partial Frequency Redistribution. This contradiction will be discussed below.

Finally, Bertaux et al. (1985) have used a third approach which is based on the following remark. The total intensity can be divided between first order scattering photons and higher orders. It is rather easy to compute the first term which includes extinction between the sun, the scattering point and the observer. However by neglecting extinction between the sun and the scattering point, one will somewhat over estimate the first term thus compensating for the lack of the second term. The main problem with this assumption is that it is not based on any actual computation.

In this section, we will present a validation of the Monte Carlo scheme by studying the line profile computation of the primary term (first order of scattering). Then we will estimate the relative importance of multiple scattering in our problem.

3.1. Validity of Monte Carlo method

In this section, we have tested the computation of the primary emissivity by the Monte Carlo approach. It is straightforward to estimate numerically the primary emissivity and its spectral dependence, as given by Eqs. (13) and (14), because all zero order photons come from the sun. On the other hand, the individual scattering process of each photon is exactly the same whatever the scattering order of the photon. Then, the compar-

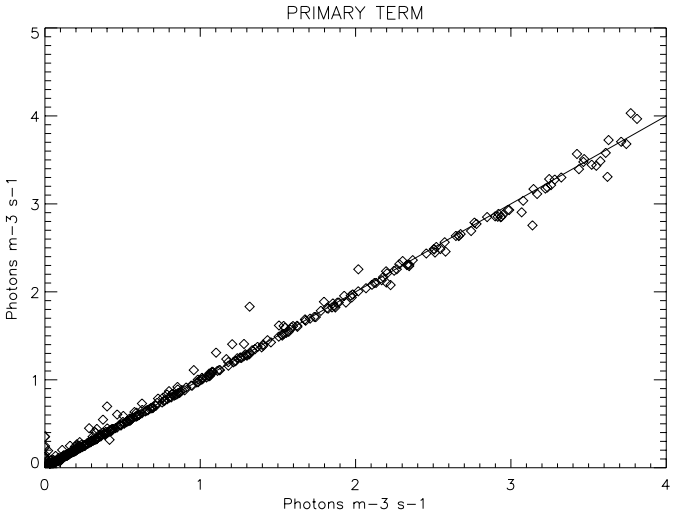

Fig. 1. Comparison of primary emissivity computed in two different ways. For each point within 200 AU from the sun we have plotted the result of the Monte Carlo simulation as a function of the numerical estimate of the emissivity. The straight line has a slope equal to 1. The hot model parameters in this simulation are $N_H = 0.15\,\mathrm{cm}^{-3}$, $V_H = 20\,\mathrm{km\,s}^{-1}$ and $T_H = 8000\,\mathrm{K}$.

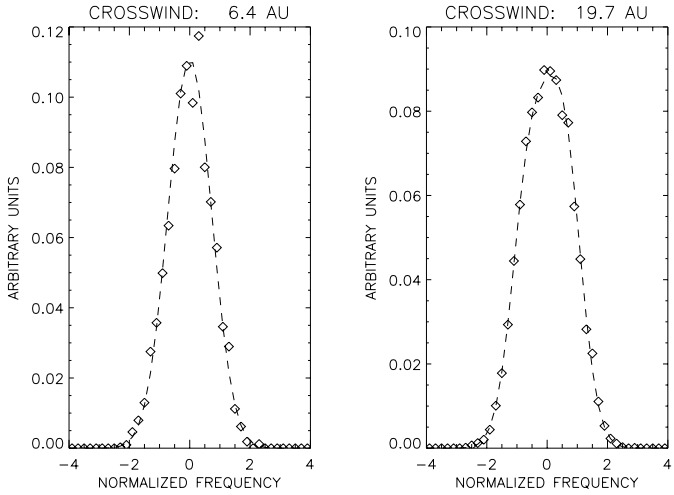

Fig. 2. Comparison of the line profile of the primary emissivity computed in two different ways. The direction of the outgoing photons is radially away from the sun. The scattering points are crosswind at 6.4 AU and 19.7 AU, respectively. Diamonds indicate the Monte Carlo simulation results. Dash marks are results from the numerical simulation. The hot model parameters in this simulation are $N_H = 0.15\,\mathrm{cm}^{-3}$, $V_H = 20\,\mathrm{km\,s}^{-1}$ and $T_H = 8000\,\mathrm{K}$.

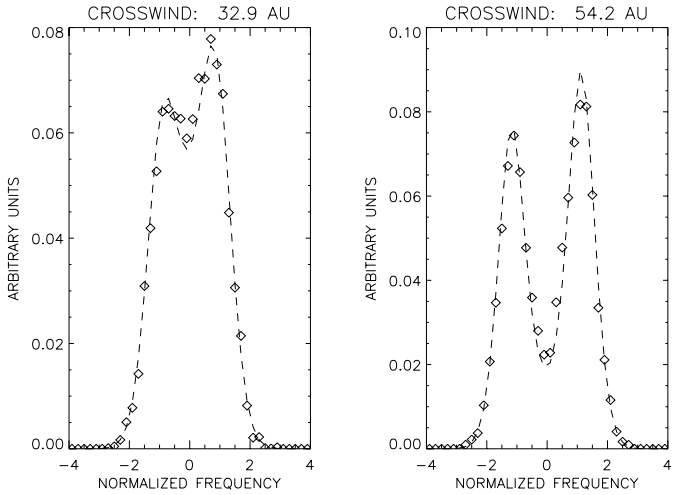

Fig. 3. Same as in the previous figure for two scattering points crosswind at 32.9 AU and 54.2 AU away from the sun. The line center reversal is due to absorption between the sun and the scattering point. The hot model parameters in this simulation are $N_H = 0.15\,\mathrm{cm}^{-3}$, $V_H = 20\,\mathrm{km\,s}^{-1}$ and $T_H = 8000\,\mathrm{K}$.

ison of the results of both methods is a good test of the Monte Carlo approach. In this test, the simulation is stopped after the first scattering. In the next sections, there will be no limit on the scattering order.

In Fig. 1, we first compare the first order emissivity (in units of $\mathrm{m}^{-3}\,\mathrm{s}^{-1}$) computed in both ways (numerically in abscissa and Monte Carlo in ordinate). This had been done in Quémerais & Bertaux (1993). Here however, the emissivity was computed in the case of Angle Dependent Partial Frequency Redistribution.

In Fig. 2, we show a comparison of the line profile of the first order emissivity computed in both ways, applying Eqs. (13) and (14) or using the Monte Carlo code. For this figure, the scattering point is crosswind at the distance shown in the label. The direction of the outgoing photons is radial and away from the sun. Fig. 3 shows the same computations for two points even farther away from the sun, i.e. 32.9 AU and 54.2 AU. These figures show that the Monte Carlo approach represents well the spectral distribution of the outgoing photon and that extinction between the sun and the scattering point which depends on the velocity distribution of the hydrogen atoms between the sun and the scattering point is correctly represented.

Table 1 gives a good example of what we call apparent temperature as opposed to the actual local temperature. For each line profile given in frequency units by $I(\nu)$, we estimate the line width by the following quantity,

$$\sigma_\nu^2 = \left(\int \nu^2\, I(\nu)\, d\nu \right) - \left(\int \nu\, I(\nu)\, d\nu \right)^2 . \qquad (18)$$

By comparison to a gaussian profile, we can define the apparent temperature of the line T_{ap} by the following expression, where c is the velocity of light in vacuum, ν_o the frequency of Lyman α transition and m_H the mass of the hydrogen atom.

$$\frac{k\,T_{ap}}{m_H} = \left(\frac{c^2}{\nu_o^2} \right) \sigma_\nu^2 . \qquad (19)$$

If we consider a hydrogen gas, with a maxwellian distribution at a temperature T, illuminated by a white source then the scattered profile will be a gaussian profile with an apparent temperature equal to the actual local temperature of the gas. But in a realistic case, the apparent temperature can be very different from the local temperature even if the source is white, i.e.

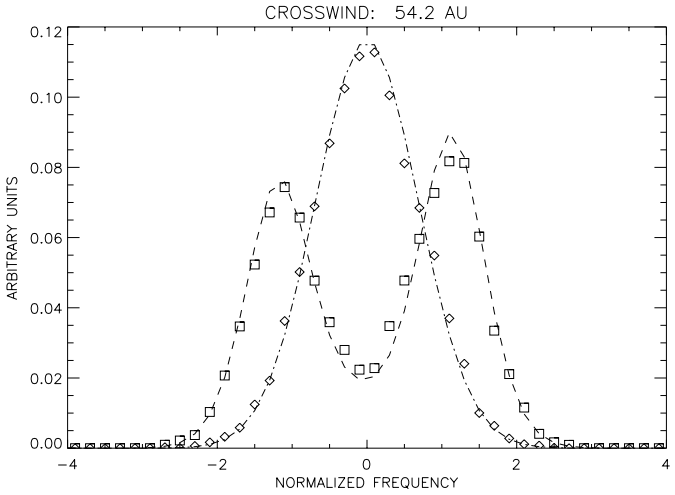

Fig. 4. Line profile of primary emissivity for a scattering point at 54.2 AU from the sun in the crosswind direction. The dash line shows the radial profile and the dash-dot line shows the perpendicular profile. The Monte Carlo results are shown by squares (radial) and diamonds (perpendicular). The hot model parameters in this simulation are $N_H = 0.15\,\mathrm{cm}^{-3}$, $V_H = 20\,\mathrm{km\,s}^{-1}$ and $T_H = 8000\,\mathrm{K}$.

Table 1. Apparent temperature of radial primary emissivity

CROSSWIND	
r (AU)	K (radial)
3.19	7998
6.35	8170
11.45	8769
19.67	10419
32.90	14489
54.20	23144

has a flat spectral profile. For instance, at large distance from the sun as in Fig. 3, extinction between the source and the scattering point creates a strong reversal at line center, Thus, the apparent temperature gives unrealistic values. This is shown by Table 1 where we give the apparent temperature of the radial local primary emissivity at various distances from the sun. In this computation, we have taken a white source and the local temperature is close to 8000 K after 5 AU. Yet, the apparent radial temperature increases dramatically due to extinction between the sun and the observer.

This effect is due to the fact that the scattering process is totally coherent when incoming and outgoing photons are colinear (see Eq. (12)). For the primary term, all photons come from the sun which means that radial scatterings are coherent. This is not the case for perpendicular scatterings. In that case, there is complete frequency redistribution which means that perpendicular local emissivity will be a gaussian profile with an apparent temperature equal to the local temperature of the gas. This is shown by Fig. 4 where we have represented a radial and a perpendicular primary emissivity profile at large distance from the sun. The radial profile is coherent and shows a strong line center reversal. The perpendicular profile is a gaussian profile at the temperature of local gas. This is obtained by both our numerical and Monte Carlo simulation.

The study of the primary emissivity has enabled us to validate the way the Monte Carlo code treats the individual scattering process both for radial and perpendicular scatterings. The strength of the Monte Carlo approach lies in the fact that the same routines are applied to compute the spectral profile whatever the scattering order of the photon.

This section shows also that the results of the ADPFR model are drastically different from the results of the CFR model where all local emissivity line profiles are gaussian profiles at the local temperature of the gas.

3.2. Can multiple scattering be neglected at 1 AU?

The aim of this section is to prove **quantitatively** that multiple scattering effects cannot be neglected anywhere in the heliosphere, even at 1 AU from the sun, even for low hydrogen number at infinity as stated in Scherer et al. (1999).

The model used here is a so-called hot model with no interface. The interstellar hydrogen distribution is defined by a bulk velocity of $20\,\mathrm{km\,s}^{-1}$ and a temperature of 8000 K. We have taken a value for the hydrogen number density equal to $0.05\,\mathrm{cm}^{-3}$ which corresponds to a lower limit of what is currently believed. Higher values of N_H will increase the relative importance of multiple scattering.

Radiative transfer effects have been computed as described above, combining a direct numerical computation for the first and second scatterings and the Monte Carlo approach for higher orders. The hydrogen distribution is described locally by its mean velocity in the solar rest frame and temperatures along 3 perpendicular axes. This distribution is used for all scatterings without any simplification. A white source has been used for the sun.

Table 2 gives the characteristic values of interest here in the case where the interstellar hydrogen number density is equal to $0.05\,\mathrm{cm}^{-3}$ for points at 6 distances from the sun along three directions, upwind, crosswind and downwind. For each point we give the distance from the sun, the optical thickness at line center, the equivalent transmission computed from the Holstein function (Holstein, 1947), and the ratio over the primary term of the emissivity of the two first scattering orders ε_1 and ε_2.

From this table, we note that for a point at 1 AU from the sun, the secondary emissivity corresponds to roughly less than 2% of the primary term. This would lead us to neglect multiple scattering effects. However this reasoning is wrong because, in that way one forgets the fact that the intensity is obtained by integration over the line of sight. This line of sight extends over more 10 AU as shown by Fig. 5. At 5 AU from the sun in the upwind direction, the secondary term corresponds to more than 25% of the primary term. At 10 AU, it is more than 75%. Although at 1 AU the interplanetary medium is optically thin at Lyman α, the contribution of the medium beyond 10 AU is still important and at that distance from the sun the interplanetary medium is optically thick at Lyman α.

Table 2. Characteristic values in the inner heliosphere

N_H = 0.05 cm^{-3}						
			UPWIND			
r in AU	1.00	2.00	5.00	10.00	20.00	50.00
τ	2.73 $\times 10^{-3}$	0.0107	0.0638	0.207	0.558	1.82
$T(\tau)$	0.998	0.992	0.956	0.865	0.682	0.319
$\varepsilon_1/\varepsilon_0$	0.0156	0.0361	0.123	0.284	0.545	0.785
$\varepsilon_2/\varepsilon_0$	0.00	0.00148	0.0480	0.178	0.809	4.34
			CROSSWIND			
r in AU	1.00	2.00	5.00	10.00	20.00	50.00
τ	7.12 $\times 10^{-4}$	3.66 $\times 10^{-3}$	0.0314	0.128	0.403	1.50
$T(\tau)$	0.999	0.997	0.978	0.914	0.757	0.380
$\varepsilon_1/\varepsilon_0$	0.0115	0.0265	0.0954	0.237	0.488	0.818
$\varepsilon_2/\varepsilon_0$	0.00	9.97 10^{-3}	0.0456	0.183	0.719	4.10
			DOWNWIND			
r in AU	1.00	2.00	5.00	10.00	20.00	50.00
τ	4.17 $\times 10^{-6}$	5.92 $\times 10^{-5}$	1.81 $\times 10^{-3}$	0.0165	0.0945	0.629
$T(\tau)$	0.999997	0.999958	0.9987	0.988	0.936	0.651
$\varepsilon_1/\varepsilon_0$	0.00640	0.0139	0.0495	0.134	0.321	0.745
$\varepsilon_2/\varepsilon_0$	0.00	0.00	0.00	0.187	0.523	2.83

Table 3. Estimates of various components of intensity at 1 AU

		ADPFR intensity	SO = 0	SO = 1	SO $\geq$ 2	O.T. ratio	S.A. ratio
0.05 cm^{-3}	UPWIND	236 R	73%	12%	15%	1.00	0.80
0.05 cm^{-3}	CROSSWIND	164 R	73%	13%	14%	0.96	0.74
0.05 cm^{-3}	DOWNWIND	53 R	44%	14%	42%	0.82	0.51
0.10 cm^{-3}	UPWIND	464 R	65%	13%	22%	1.02	0.74
0.10 cm^{-3}	CROSSWIND	330 R	57%	14%	29%	0.95	0.65
0.10 cm^{-3}	DOWNWIND	118 R	34%	13%	53%	0.74	0.40
0.15 cm^{-3}	UPWIND	684 R	60%	14%	26%	1.03	0.70
0.15 cm^{-3}	CROSSWIND	493 R	52%	14%	34%	0.96	0.60
0.15 cm^{-3}	DOWNWIND	184 R	29%	12%	59%	0.72	0.35

Table 3 gives quantitative values for the various components contributing to the total intensity as seen at 1 AU looking radially. The computation has been made for 3 different values of the interstellar hydrogen number density. In the best case, i.e. upwind for 0.05 cm^{-3}, the primary term corresponds to 73% of the total intensity. Photons with order of scattering equal to 2 or higher still represent 15% of the total intensity. The last two columns give the ratio of the optically thin case result (O.T.) divided by the radiative transfer result and of the case with Self-Absorption divided by the radiative transfer result. We call self-absorption (S.A.) the case where extinction between the scattering point and the observer is taken into account.

4. Comparison with CFR hypothesis

In this section, we are comparing the results of our present computation with a previous work made by Quémerais & Bertaux (1993). These authors have developed a code based on a Monte Carlo approach assuming Complete Frequency Redistribution. The gas was assumed isothermal with a constant velocity everywhere in the heliosphere. Because of these assumptions, it was impossible to compute actual Lyman α background line profiles. However, as it appears here, the multiple scattering effects on the total emissivity were correctly represented.

Fig. 6 shows a comparison of both CFR and ADPFR multiple scattering computations made with the same hydrogen distribution ($V_H = 20$ km s^{-1}, $T_H = 8000$ K and three values for N_H, 0.05 cm^{-3}, 0.10 cm^{-3} and 0.15 cm^{-3}). In both cases the solar source is white and there is no scattering phase function because the work of Quémerais & Bertaux (1993) did not include it. The ADPFR computation uses additionally actual velocity and temperature distributions everywhere in the heliosphere.

This figure shows that there is a good agreement between CFR and ADPFR computations in terms of number of photons backscattered in the inner heliosphere. For a study of intensity measurements, one could easily restrict the computation to the CFR assumption which is much simpler. However, ADPFR becomes necessary to study actual line profiles.

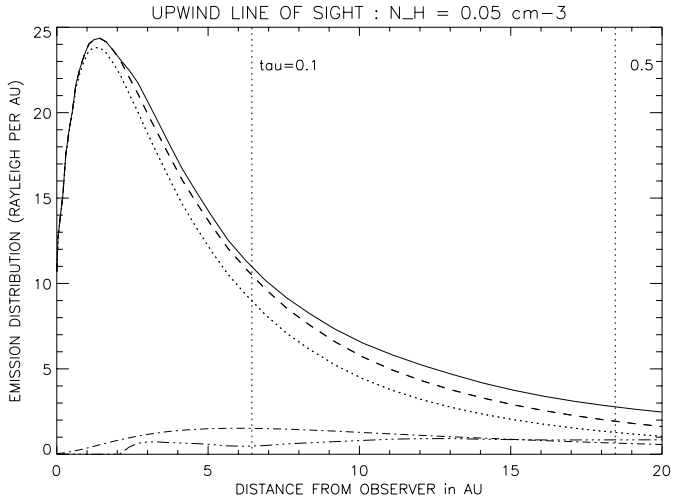

Fig. 5. Emission distribution in Rayleigh per AU for an observer at 1 AU in the upwind direction looking radially away from the sun. The solid line shows the total (ADPFR) intensity. The dotted line corresponds to the primary term and the dashed line to the photons with order of scattering equal to one (see text). The peak is at 2 AU from the observer. The contribution at 10 AU is still 25% of the peak contribution. The primary term corresponds only to 73% of the total intensity. This fraction is even smaller for higher values of N_H, which proves that multiple scattering effects cannot be neglected even close to the sun.

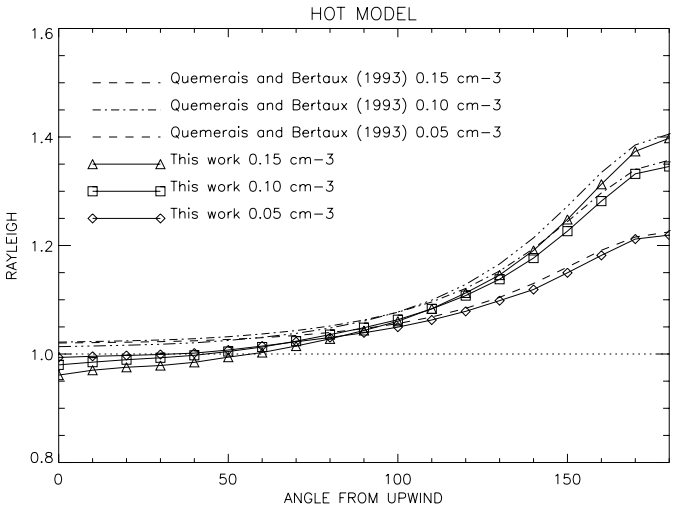

Fig. 6. Plot of the ratio of the multiple scattering intensity over the optically thin approximation as a function of angle with the upwind direction. The observer is at 1 AU and is looking radially away from the sun. The dash-dot lines are from Quémerais & Bertaux (1993) assuming CFR. There is a good agreement between CFR and ADPFR when one considers the effects of multiple scattering on the total number of photons. The small difference in the two computational methods comes from the inclusion of mean velocities and temperatures in the ADPFR model.

5. Lyman α background in the heliosphere

This section will detail the results of our Angle Dependent Partial Frequency Redistribution computations for a hot model. This study does not take the interface into account, so the results in the outer heliosphere will be very different from what would be obtained from interface models.

In what follows, the observer is looking radially away from the sun. The zero and first order scatterings are computed numerically from above. The other scatterings are computed via the Monte Carlo code. All the computations include the classical phase function established by Brandt and Chamberlain (1959).

First, we will show the results for a white solar source in both the inner and the outer heliosphere. Then we will use a realistic solar source. The solar parameters are μ, the ratio of radiation pressure over solar gravitation equal to 1 and the hydrogen lifetime against ionization at 1 AU equal to 1.2×10^6 seconds. These are standard values for an isotropic hot model. The hydrogen distribution depends also on the interstellar parameters. The hydrogen number density distribution is proportional to N_H, the value of the hydrogen number density at large distance from the sun. In this study, we have used three values for N_H, 0.07, 0.12 and 0.17 cm^{-3}, which covers the range of possible values commonly accepted (Quémerais et al., 1994). We have also used three different values for V_H (20, 22 and 26 km s^{-1}) and T_H (6000, 8000 and 10 000 K).

5.1. Lyman α background in the inner heliosphere

Recently, Quémerais et al. (1999) and Lallement et al. (1999) have studied the SWAN/SOHO H cell measurements to try to derive the velocity and temperature distribution as seen from 1 AU. Although the study of Costa et al. (1999) did not include multiple scattering, they estimated that the mean shifts and line widths measured by SWAN were compatible with a hot model defined by $V_H = 22$ km s^{-1} and $T_H \approx 11\,000$ K.

Here, we have taken a hot model with the solar parameters given above and with $V_H = 22$ km s^{-1} and $T_H = 10\,000$ K. Three possible values for N_H were used also.

Table 4 shows the results of the ADPFR computation for an observer at 1 AU from the sun and looking radially away from the sun. For each values of N_H, we give the total intensity (I_n), the mean shift of the line (V_n) in the solar rest frame and the apparent temperature (T_n).

As pointed out before, the values for the intensity found here are close to the results obtained by CFR for the same hydrogen distribution. We note also that the upwind to downwind intensity ratio is affected by the value of N_H. This ratio goes from 4.4 to 4.0 as the number density changes from 0.07 to 0.17 cm^{-3}. With a larger density, we have more multiple scattering and a relatively more efficient filling of the cavity (Quémerais & Bertaux, 1993). From Table 4, we see that the line shifts are not much affected by the actual value of N_H. This model gives an apparent velocity at 1 AU equal to -25 km s^{-1} in the upwind direction and equal to close to 21 km s^{-1} in the downwind direction. Finally, we see also that the apparent temperature increases when N_H increases. Derivation of the interstellar temperature is rather sensitive to effects of multiple scattering. A good knowledge of N_H is necessary if we want to correct the apparent temperatures measured by SWAN for effects of multiple scattering.

Table 4. Inner background intensity, mean shift and apparent temperature

	HOT MODEL			$V_H = 22\,\mathrm{km\,s^{-1}}$			$T_H = 10\,000$ K		
	$N_H = 0.07\,\mathrm{cm^{-3}}$			$N_H = 0.12\,\mathrm{cm^{-3}}$			$N_H = 0.17\,\mathrm{cm^{-3}}$		
θ	I_n	V_n	T_n	I_n	V_n	T_n	I_n	V_n	T_n
(°)	(R)	($\mathrm{km\,s^{-1}}$)	(K)	(R)	($\mathrm{km\,s^{-1}}$)	(K)	(R)	($\mathrm{km\,s^{-1}}$)	(K)
0	412	-25.0	10330	698	-25.1	11208	967	-25.2	11729
10	408	-24.7	10452	689	-24.8	11212	965	-24.8	11549
20	403	-23.6	10649	681	-23.7	11251	950	-23.8	11824
30	395	-22.0	10812	669	-22.0	11448	929	-22.0	11962
40	384	-19.7	10945	649	-19.7	11584	907	-19.8	12108
50	368	-16.9	11146	625	-17.0	11795	870	-17.0	12323
60	352	-13.7	11294	596	-13.7	11957	833	-13.8	12485
70	333	-10.0	11504	562	-10.1	12266	784	-10.1	12722
80	310	-6.2	11720	526	-6.2	12492	734	-6.3	12996
90	285	-2.3	11920	485	-2.3	12676	681	-2.3	13205
100	257	1.7	12111	442	1.7	12843	621	1.7	13404
110	232	5.6	12191	398	5.6	12988	560	5.5	13503
120	204	9.2	12243	352	9.2	13030	498	9.2	13626
130	177	12.5	12321	309	12.5	13142	436	12.4	13755
140	152	15.4	12293	265	15.3	13252	379	15.3	13862
150	129	17.7	12457	227	17.6	13467	324	17.6	14131
160	110	19.4	12630	197	19.3	13687	282	19.3	14556
170	97	20.5	12754	177	20.3	13771	254	20.5	14790
180	93	20.7	12761	170	20.8	13726	239	20.6	14777

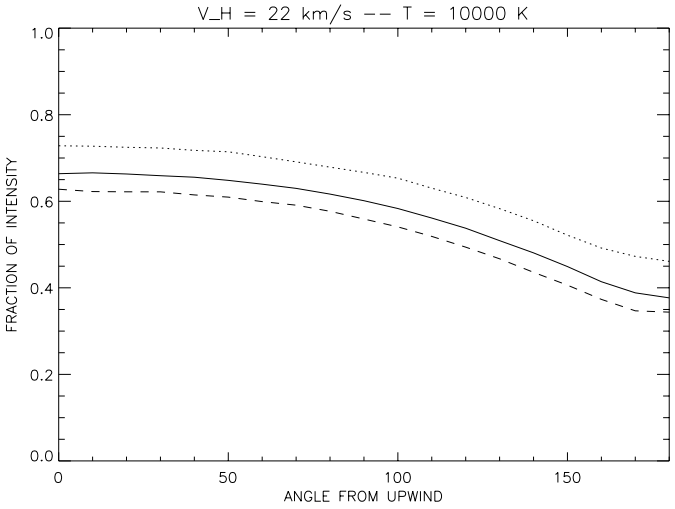

Fig. 7. Ratio of the intensity computed by taking only the primary term into account divided by the intensity deduced from the ADPFR computation as a function of the angle from the upwind position. The observer is at 1 AU looking radially away from the sun. The dashed line corresponds to $N_H = 0.17\,\mathrm{cm^{-3}}$, the solid line to $N_H = 0.12\,\mathrm{cm^{-3}}$ and the dotted line to $N_H = 0.07\,\mathrm{cm^{-3}}$. This shows that even for low values of N_H the primary term approximation fails to represent correctly the total intensity.

Table 5 has been computed for a hydrogen distribution defined by $N_H = 0.12\,\mathrm{cm^{-3}}$, $V_H = 22\,\mathrm{km\ s^{-1}}$ and $T_H = 10\,000$ K. The aim of this table is to compare the results of the ADPFR multiple scattering computation with the results of the three approximations described above. The first one used by Scherer et al. (1999) takes only the primary term into account. Here the results will be noted I_0, V_0 and T_0. The second approximation is the true optically thin approximation, noted I_{ot}, V_{ot} and T_{ot}. The third approximation used by Bertaux et al. (1985), and recently by Costa et al. (1999), adds extinction between the scattering point and the observer. This is the so-called self-absorption approximation, noted I_a, V_a and T_a.

The first three columns show intensity ratios. As found by Keller et al. (1981), Hall (1992) or Quémerais & Bertaux (1993), the optically thin approximation is quite correct in the upwind direction. There is a 20% discrepancy in the downwind direction due to the so-called partial filling of the cavity by radiative transfer effects. The primary term fails here because as we noted earlier the cavity is an optically thin medium surrounded by an optically thicker medium which sends photons back. Fig. 7 shows the intensity ratio of the primary term over the multiple scattering computation as a function of the angle to the upwind direction. The line corresponds to the values of the first column of Table 5. The dashed line shows the same ratio in the case of $N_H = 0.17\,\mathrm{cm^{-3}}$ and the dotted line is for $N_H = 0.07\,\mathrm{cm^{-3}}$.

Columns 4 to 6 of Table 5 give the difference of line mean shift in $\mathrm{km\ s^{-1}}$. This shows that the mean shift is best represented by the optically thin approximation. However, all approximations give values within $1\,\mathrm{km\,s^{-1}}$ of the ADPFR result.

Columns 7 to 9 of Table 5 give the ratios of the apparent temperature of the line profiles. In that case, the best result is obtained by the primary term and the worst by the optically thin approximation.

In conclusion, we see that the optically thin approximation is better to estimate the number of backscattered photons. On the

Table 5. Comparison of Multiple Scattering to Various Approximations

	$N_H = 0.12\,\mathrm{cm}^{-3}$			$V_H = 22\,\mathrm{km\,s}^{-1}$			$T_H = 10\,000$ K		
θ	I_0/I_n	I_{ot}/I_n	I_a/I_n	$V_0 - V_n$	$V_{ot} - V_n$	$V_a - V_n$	T_0/T_n	T_{ot}/T_n	T_a/T_n
0	0.66	1.04	0.75	-0.68	0.20	-0.46	0.91	0.81	0.88
10	0.67	1.05	0.76	-0.70	0.18	-0.48	0.92	0.82	0.89
20	0.66	1.04	0.75	-0.79	0.08	-0.58	0.92	0.82	0.89
30	0.66	1.04	0.75	-0.78	0.08	-0.57	0.92	0.82	0.89
40	0.66	1.04	0.74	-0.75	0.10	-0.54	0.93	0.82	0.90
50	0.65	1.03	0.74	-0.71	0.13	-0.50	0.94	0.82	0.91
60	0.64	1.03	0.73	-0.68	0.15	-0.48	0.95	0.83	0.92
70	0.63	1.02	0.72	-0.67	0.13	-0.47	0.95	0.82	0.92
80	0.62	1.01	0.70	-0.67	0.11	-0.48	0.96	0.82	0.92
90	0.60	1.00	0.69	-0.58	0.18	-0.39	0.97	0.82	0.93
100	0.58	0.99	0.67	-0.57	0.16	-0.40	0.98	0.82	0.94
110	0.56	0.97	0.65	-0.53	0.17	-0.37	0.98	0.82	0.94
120	0.54	0.95	0.62	-0.48	0.19	-0.32	1.00	0.82	0.95
130	0.51	0.93	0.59	-0.43	0.21	-0.28	1.00	0.82	0.95
140	0.48	0.91	0.56	-0.36	0.25	-0.22	1.00	0.81	0.95
150	0.45	0.88	0.53	-0.32	0.27	-0.19	0.99	0.80	0.94
160	0.41	0.84	0.49	-0.22	0.35	-0.10	0.97	0.78	0.92
170	0.39	0.82	0.46	-0.16	0.40	-0.05	0.97	0.77	0.92
180	0.38	0.81	0.45	-0.28	0.27	-0.17	0.98	0.78	0.92

other hand, the line profile is better approximated by computing the primary term. The numerical values presented here give estimates on the errors made by using one of the approximations.

5.2. Lyman α background in the outer heliosphere

In this section we present results of the hot model in the outer heliosphere. Effects of the interface have not been included here. This will be presented in future works. Here, we will focus on the effects on the intensity, line shift and line width due to an increasing distance from the sun.

No approximation can be used to describe the intensity away from the inner heliosphere. Fig. 8 is an illustration of this statement. This shows a computation of the intensity for an observer upwind at different distances from the sun and looking radially away from the sun. All approximations, except optically thin, fall down much faster than the multiple scattering value. Since there is no extinction, the optically thin approximation overestimates the correct decrease of intensity. It must be noted that for our model here, the density distribution outside 30 AU is more or less constant. In that case, the optically thin approximation falls off like $1/r$ and the radiative transfer case falls off like $1/r^{\alpha}$, where α is a coefficient between 1 and 2 (Hall, 1992). The coefficient α depends on the optical thickness of the medium, i.e. on the value of N_H and distance from the sun. When an interface is included the upwind hydrogen number density shows a positive gradient in the outer heliosphere (Baranov & Malama, 1993). In that case, α can be smaller than 1. This is why measuring the fall-off of the upwind intensity from the Voyager UVS data is important (Hall et al., 1993; Quémerais et al., 1996).

In the downwind direction (Fig. 9), the situation is more complex. The hydrogen cavity extends much farther from the sun and even at 60 AU the hydrogen number density has not reached a constant value. The size of the cavity is affected by the solar parameters and its filling by the mean velocity and temperature of the interstellar gas. Study of the downwind interplanetary background as a function of solar distance is then more dependent on the solar and interstellar parameters. It is also strongly affected by the variability of the solar parameters (Ruciński & Bzowski, 1995).

Fig. 10 shows how the upwind profile mean shift (apparent velocity) changes with solar distance. This has been computed

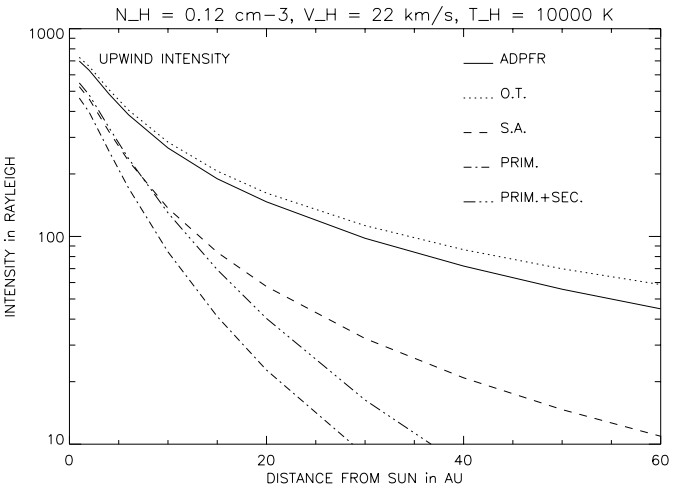

Fig. 8. Upwind radial intensity as a function of solar distance between 1 and 60 AU. After 30 AU, the optically thin approximation falls off like $1/r$. The radiative transfer computation follows $1/r^{\alpha}$ where $1 \leq \alpha \leq 2$, depending on the optical thickness of the medium. The other computations decrease very quickly with solar distance.

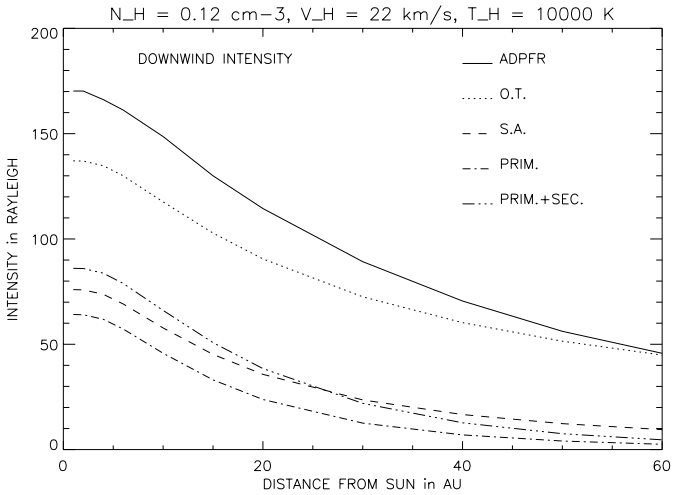

Fig. 9. Downwind radial intensity as a function of solar distance between 1 and 60 AU. Here the situation is much more complex than in the upwind direction because even at 60 AU the H number density is not constant. We see also that multiple scattering effects are predominent.

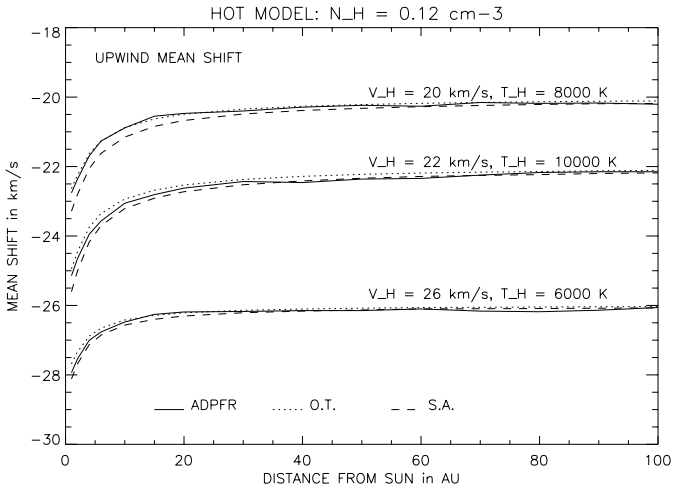

Fig. 10. Mean shift of the line profile obtained for an observer looking radially away from the sun in the upwind direction. In the case of the hot model, at large distance from the sun, the shift is equal to the velocity of the interstellar gas. The shifts have been computed for three types of models with V_H =20, 22 and 26 km s^{-1}. At one AU in the upwind direction, the apparent velocities found for each model are -22.8 km s^{-1}, -25.1km s^{-1} and -27.9 km s^{-1}, respectively.

for three different values of V_H, namely 20, 22 and 26 km s^{-1}. We see that the apparent velocity of the line seems to increase by roughly 3 km s^{-1} in the inner heliosphere. This is caused by the apparent acceleration of the hydrogen atoms due to selection effects (here $\mu = 1$, so there is no gravitational acceleration). Slower atoms are more easily ionized because they spend more time near the sun. This results in a selection of faster atoms and an increase of the local mean velocity, i.e. an apparent acceleration. Note that the value found by Quémerais et al. (1999) of 25.3 km s^{-1} for the apparent velocity measured in the upwind direction at one AU is consistent with a model with 22 km s^{-1} at large distance from the sun.

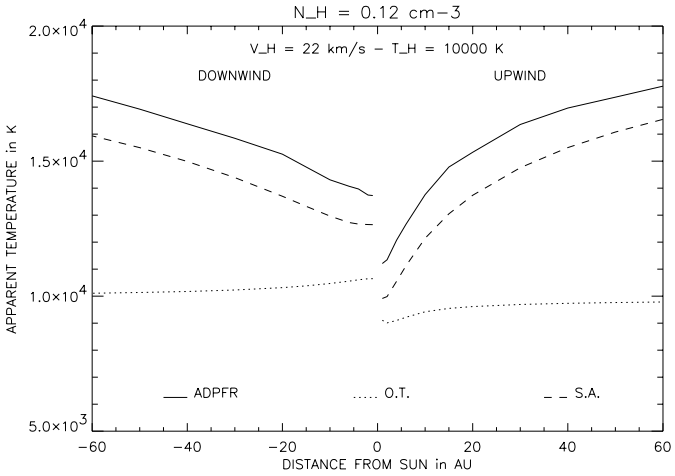

Fig. 11. Apparent temperature of line profiles obtained for an observer looking radially away from the sun. The values are shown in both the upwind and downwind directions. The dotted line gives the result of the optically thin approximation, the solid line the ADPFR result and the dashed line corresponds to the computation of the self-absorbed case.

Fig. 11 shows the apparent temperature in both the upwind and downwind directions as a function of distance from the sun. On this figure, we show the results for the optically thin approximation (dotted line), the ADPFR radiative transfer (solid line) and the self-absorbed computation (dashed line). The primary term is not shown here because the extinction near line center makes the estimation of the apparent temperature completely unrealistic. First, we note that the optically thin approximation strongly underestimates the apparent temperature. It goes asymptotically back to the value of the gas in the interplanetary medium. Self-absorption gives the value closest to the actual result of ADPFR although the results are systematically underestimated by roughly 1000 K. At very large distance from the sun, the apparent temperature is a complex mixture of coherent and perpendicular scatterings. We know that perpendicular scatterings have an apparent temperature equal to the temperature of the medium. On the other hand, after many scatterings the profile of the photons which are scattered is not white anymore. In an extreme case, let us assume that after n scatterings the source profile for the $n + 1$ scattering is a doppler profile at the temperature of the gas. Then because we assume a doppler scattering cross section, the coherently scattered profile has an apparent temperature which is half the actual temperature of the gas. The total emissivity will be a complex mixture of these various profiles. The widening of the line is mainly driven by extinction when integrating over the line of sight. A gaussian profile at temperature T attenuated following a gaussian at the same temperature yields an apparent temperature which is larger than the original one. All these antagonist effects are taken into account in our computation. Finally, the variation of the Lyman α line profile with distance depends strongly on the optical thickness in the interplanetary medium, hence of the parameter N_H.

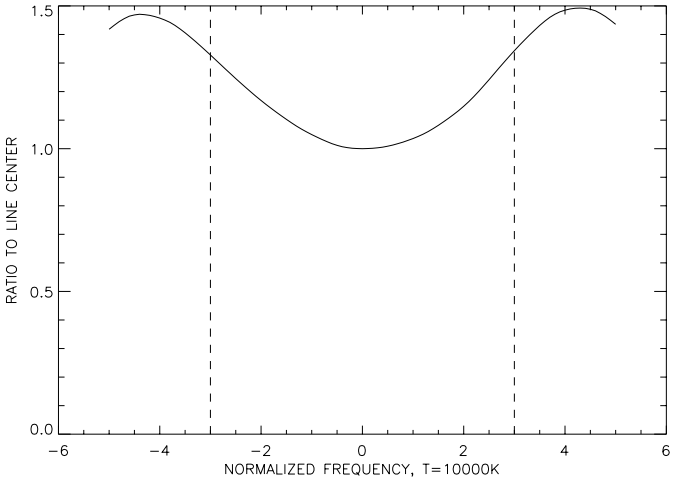

Fig. 12. Solar profile used in this computation as a function of doppler width. It has been measured by SUMER on SOHO in 1996. The normalized frequency has been computed for 10 000 K. At two doppler widths from line center the flux is 20% higher than in the line center. At three doppler widths (dashed lines), it is 30% higher. Photons outside 5 doppler widths are neglected from this computation.

5.3. Using a realistic solar profile

In this last section, we will present results obtained when the spectral distribution of the solar photons is realistically represented.

The solar H Lyman α line profile used here has been obtained by the SUMER instrument on SOHO (Lemaire et al., 1998). Its main feature is that the central reversal of the line has a strong parabolic shape which means that there will be more photons emitted in the wings of the line. One difficulty arises here. Due to the uncertainty in the SUMER absolute wavelength calibration, we had to assume that the center of the reversal corresponds to the actual line center in the solar rest frame. This may be inexact.

Fig. 12 shows this solar photons spectral distribution. On this figure, we have marked the limit of three doppler widths (for a gas at 10 000 K) from line center. We see that at this distance from solar center the flux is 30% higher. This has a first consequence on intensity measurements. We know that in the upwind direction the mean shift of H atoms is 20 to 25 km s^{-1} in the solar rest frame. A similar effect exists also downwind. On the other hand the radial shift crosswind is close to zero. This means that atoms in the crosswind area will be predominently lit by a line center flux whereas upwind and downwind atoms will see a flux close to two doppler widths away from line center, i.e. some 20% higher. This will make both upwind and downwind regions brighter than in a case of a spectrally flat initial source.

This is shown quantitatively in Table 6 where we show the ratios for $N_H = 0.12\,\mathrm{cm}^{-3}$ of the computation using the SUMER profile (I_s) over the white profile (I_w). The ratio has been computed for the ADPFR case and for the approximations as well. On all cases, we see that upwind and downwind regions are relatively brighter.

Table 6. Intensity Ratio of Solar Type Source to White Source

0.12 cm^{-3}, 22 km s^{-1}, 10 000 K				
θ (°)	$(I_s/I_w)_n$	$(I_s/I_w)_0$	$(I_s/I_w)_{ot}$	$(I_s/I_w)_a$
0	1.15	1.18	1.17	1.18
10	1.15	1.18	1.17	1.17
20	1.14	1.17	1.15	1.16
30	1.12	1.15	1.14	1.15
40	1.11	1.13	1.12	1.13
50	1.10	1.10	1.09	1.10
60	1.07	1.08	1.07	1.08
70	1.06	1.06	1.05	1.06
80	1.05	1.04	1.03	1.04
90	1.04	1.03	1.02	1.03
100	1.04	1.03	1.02	1.02
110	1.04	1.03	1.03	1.03
120	1.05	1.04	1.04	1.04
130	1.06	1.06	1.05	1.06
140	1.07	1.07	1.07	1.07
150	1.08	1.09	1.09	1.09
160	1.08	1.11	1.10	1.11
170	1.09	1.12	1.11	1.12
180	1.08	1.12	1.12	1.12

Table 7. Mean Shift Variation (δV in km s^{-1}) – Solar Type Source to White Source

0.12 cm^{-3}, 22 km s^{-1}, 10 000 K				
θ (°)	$(\delta V)_n$	$(\delta V)_0$	$(\delta V)_{ot}$	$(\delta V)_a$
0	-0.58	-0.74	-0.66	-0.71
10	-0.58	-0.74	-0.66	-0.71
20	-0.58	-0.73	-0.65	-0.71
30	-0.51	-0.72	-0.64	-0.70
40	-0.49	-0.70	-0.61	-0.68
50	-0.40	-0.66	-0.57	-0.64
60	-0.32	-0.59	-0.50	-0.57
70	-0.30	-0.48	-0.40	-0.46
80	-0.23	-0.34	-0.28	-0.32
90	-0.07	-0.17	-0.13	-0.16
100	-0.01	0.02	0.03	0.03
110	0.08	0.22	0.19	0.21
120	0.19	0.40	0.34	0.38
130	0.28	0.56	0.46	0.53
140	0.32	0.69	0.56	0.66
150	0.29	0.79	0.64	0.75
160	0.33	0.86	0.69	0.82
170	0.31	0.90	0.71	0.86
180	0.33	0.92	0.72	0.87

Table 7 shows the difference of the line mean shifts in terms of km s^{-1} in the sun rest frame ($\delta V = V_s - V_w$). From Table 7, we see that the line shifts are not much affected, all values are within 1 km s^{-1}. The reversed shape of the solar line mentioned above tends to increase the apparent velocity in both upwind and downwind direction because faster atoms see a higher flux. Perpendicularly to the upwind direction, there is little visible effect.

Table 8. Apparent Temperature Ratio - Solar Type Source to White Source

$0.12\,\mathrm{cm}^{-3}$, $22\,\mathrm{km\,s}^{-1}$, 10 000 K				
θ (°)	$(T_s/T_w)_n$	$(T_s/T_w)_0$	$(T_s/T_w)_{ot}$	$(T_s/T_w)_a$
0	1.00	1.00	1.00	1.00
10	1.01	1.00	1.01	1.00
20	1.02	1.00	1.01	1.00
30	1.01	1.00	1.01	1.00
40	1.01	1.01	1.01	1.01
50	1.02	1.01	1.02	1.02
60	1.02	1.02	1.03	1.02
70	1.02	1.03	1.03	1.03
80	1.02	1.04	1.04	1.04
90	1.03	1.04	1.04	1.04
100	1.03	1.04	1.04	1.04
110	1.03	1.04	1.04	1.04
120	1.03	1.04	1.04	1.04
130	1.02	1.04	1.04	1.04
140	1.02	1.04	1.03	1.04
150	1.01	1.04	1.03	1.04
160	1.02	1.03	1.03	1.03
170	1.03	1.03	1.03	1.03
180	1.03	1.03	1.03	1.03

Finally, Table 8 shows that there is a small increase of the line profiles due to the solar flux spectral distribution. This increases the apparent temperature by 4% at most meaning that the line width is increased by less than 2%. In general, the effect is not really significant. This effect could be increased if the interplanetary gas has a higher temperature.

6. Discussion

In this work, we have presented the results of a radiative transfer code which allows us to compute Lyman α background line profiles in a precise way. This code uses a Monte Carlo approach to compute the spectral distribution of photons for a scattering order higher than 1. The zero and first order of scattering are computed numerically from the explicit expression of the scattered line profile obtained from Angle Dependent Partial Frequency Redistribution.

This code can be applied to study the data of various recent measurements performed by SWAN on SOHO (Bertaux et al., 1995) and GHRS on Hubble Space Telescope (Clarke et al., 1995). New precise measurements of the interplanetary Lyman α line profile will be available also from future experiments like SCARI (Chakrabarti et al., 1994).

The first result we wish to point out here is that our code shows that multiple scattering effects cannot be neglected even in the close vicinity of the sun. This is in contradiction with the results of Scherer & Fahr (1996) and we have given quantitative results to justify this. We have compared systematically the results of our ADPFR multiple scattering code with the different approximations used by various authors.

We have found also that the Complete Frequency Redistribution (CFR) multiple scattering intensities are very close to the ones found in the case of ADPFR. This justifies the assumptions made by Keller et al. (1981), Hall (1992) and Quémerais & Bertaux (1993). However, computing the actual line profile requires a full ADPFR computation.

Finally, we have shown typical results for intensity, apparent velocity and apparent temperature both in the inner and the outer heliosphere. These were compared to various approximations. Tables of correction terms depending on line of sight direction are given here. It must be noted also that the results presented here are derived from typical hot model hydrogen distributions. We expect that the inclusion of effects of the heliospheric interface on the hydrogen distribution, as obtained by Baranov & Malama (1993) for instance, will modify the line shapes in a dramatic fashion, especially in the outer heliosphere. In that respect, the previous section on outer heliosphere Lyman α background must be taken as a study case. Hall et al. (1993) or Quémerais et al. (1995) have shown that the UVS data in the outer heliosphere do not agree with the results of hot model type computations.

Finally, the goal of this work was to present a computation method and give general conclusions for typical observations. However, making detailed comparisons with actual measurements is far beyond the scope of this paper. It will be presented in future works.

Acknowledgements. The author wishes to thank R. Lallement and J.L. Bertaux for their continuing support and advice in the development of this model.

References

Ajello J.M., Stewart A.I.F., Thomas G.E., Graps A., 1987, ApJ 317, 964
Baranov V.B., 1990, Space Sci. Rev. 52, 89
Baranov V.B., Malama Y.G., 1993, J. Geophys. Res. 98, 15157
Baranov V.B., Izmodenov V.V., Malama Y.G., 1998, J. Geophys. Res. 103, 9575
Bertaux J.L., Blamont J.E., 1971, A&A 11, 200
Bertaux J.L., Lallement R., Kurt V.G., Mironova E.N., 1985, A&A 150, 1
Bertaux J.L., Kyrölä E., Quémerais E., et al., 1995, Solar Physics 162, 403
Bertaux J.L., Lallement R., Quémerais E., et al., 1996, Space Sci. Rev. 78, 317
Bertaux J.L., Quémerais E., Lallement R., et al., 1997, Solar Physics 175, 737
Bertaux J.L., Kyrölä E., Quémerais E., al., 1999a, Space Sci. Rev. 87, 129
Bertaux J.L., Quémerais E., Lallement R., et al., 1999b, Geophys. Res. Let. 27, 1331
Brandt J.C., Chamberlain J.W., 1959, ApJ 130, 670
Brasken M., Kyrölä E., 1998, A&A 332, 732
Chakrabarti S., Cotton D.M., Vickers J.S., et al., 1994, Applied Optics 33, 2596
Clarke J.T., Lallement R., Bertaux J.L., et al., 1995, ApJ 499, 482
Costa J., Lallement R., Quémerais E., et al., 1999, A&A 349, 660
De Toma G., Quémerais E., Sandel B.R., 1997, ApJ 491, 980
Hall D.T., 1992, Ph.D. Thesis, University of Arizona, Tucson
Hall D.T., Shemansky D.E., Judge D.L., Gangopadhyay P., Gruntman M.A., 1993, J. Geophys. Res. 98, 15185

Holstein T., 1947, Physical Review 72, 1212
Keller H.U., Richter K., Thomas G., 1981, A&A 102, 415
Kyrölä E.T., Summanen W., Schmidt T., et al., 1998, J. Geophys. Res. 103, 14523
Lallement R., Bertaux J.L., Dalaudier F., 1985, A&A 150, 21
Lallement R., the SWAN team, 1999, In: Habbal, et al. (eds.) Solar Wind 9, AIP conference proceedings 471, p. 205
Lemaire P., Emerich C., Curdt W., et al., 1998, A&A 334, 1095
Mihalas D., 1970, In: Stellar Atmospheres. W.H. Freeman Co, San Francisco
Pryor W.R., Ajello J.M., Barth C.A., et al., 1992, ApJ 394, 363
Quémerais E., Bertaux J.L., 1993, A&A 277, 283
Quémerais E., Bertaux J.L., Sandel B.R., Lallement R., 1994, A&A 290, 941
Quémerais E., Sandel B.R., Lallement R., Bertaux J.L., 1995, A&A 299, 249
Quémerais E., Malama Y.U., Sandel B.R., 1996, A&A 308, 279
Quémerais E., Bertaux J.L., Lallement R., et al., 1999, J. Geophys. Res. 104, A6, 12585
Ruciński D., Bzowsli M., 1995, A&A 296, 248
Scherer U., Fahr H.J., 1996, A&A 309, 957
Scherer U., Bzowski M., Fahr H.J., et al., 1999, A&A 342, 601
Stephan S.G., Chakrabarti S., Cook T., et al., 1998, Eos Transactions, AGU volume 79, number 45, F702 (1998 AGU Fall Meeting).
Thomas G.E., Krassa R.F., 1971, ApJ 134, 20
Thomas G.E., 1978, Ann. Rev. Earth Planet. Sci. 6, 173
Zank G.P., Pauls H.L., Williams L.L., et al., 1996, J. Geophys. Res. 101, 21